Chemical Engineering Journal 424 (2021) 130316

Contents lists available at ScienceDirect

Chemical Engineering Journal

journal homepage: www.elsevier.com/locate/cej

Fluorinated quinone derived organosulfur copolymer cathodes for long-cycling, thermostable and flexible lithium–sulfur batteries

Wen Yan [a,b,1], Kun-Yun Yan [c,1], Gui-Chao Kuang [c,*], Zhong Jin [a,b,*]

[a] MOE Key Laboratory of Mesoscopic Chemistry, MOE Key Laboratory of High Performance Polymer Materials and Technology, Jiangsu Key Laboratory of Advanced Organic Materials, School of Chemistry and Chemical Engineering, Nanjing University, Nanjing 210023, China
[b] Shenzhen Research Institute of Nanjing University, Shenzhen 518063, China
[c] State Key Laboratory of Power Metallurgy, Central South University, Changsha, Hunan 410083, China

ARTICLE INFO

Keywords:
Lithium–sulfur batteries
Polymeric cathode materials
Organosulfur copolymers
Shuttle effect
Thermostability and flexibility

ABSTRACT

Organosulfur copolymers are promising cathode materials in lithium–sulfur batteries because of adjustable molecular structure, tunable electrochemical properties and excellent processability. However, conventional organosulfur copolymers suffer from poor electronic/ionic conductivity and low sulfur content, which limit rate capability and energy density. Herein, fluorinated quinone-derived organics are copolymerized with sulfur via convenient nucleophilic aromatic substitution (S_NAr) reaction. The homogeneous distribution of sulfur over poly (tetrafluorohydroquinone)-sulfur (PTFHQS) at molecular level endows excellent Li^+ ion diffusivity and fast redox kinetics. The abundant semi-ionic C–F bonds with polar characteristic have strong interactions with polysulfides, thus diminishing the shuttle effect. In result, flexible PTFHQS cathode with ~ 71 wt% sulfur content exhibits high discharge capacity of 643 mAh g^{-1}_{total} (906 mAh g^{-1}_{sulfur}) at 0.5C, stable Coulombic efficiency (>99%), good rate performance of 307 mAh g^{-1}_{total} (432 mAh g^{-1}_{sulfur}) 2.0C, excellent cycling stability (capacity retention of 87% for 600cycles), and functions normally at elevated working temperature (80 °C). Compared to another copolymer of sulfurized tetrafluoro-p-benzoquinone monomer (TFBQS), molecular structure characterization and electrochemical analysis verifies that pre-polymerized skeleton of PTFHQS is conducive to the homogeneous distribution and efficient utilization of sulfur species. We expect this work will bring inspiration to exploit organosulfur compounds with rational molecular structures and convenient synthesis routes for lithium–sulfur batteries.

1. Introduction

Lithium–sulfur (Li–S) batteries have received extensive attention due to the high theoretical energy density (2600 Wh kg^{-1}), low cost and environment friendly nature[1–4]. However, the commercial application of Li–S batteries is hindered by the strong electronic insulation of elemental sulfur and Li_2S_2/Li_2S, the shuttle effect of Li_2S_x ($4 \leq x \leq 8$) intermediates, and the severe volume expansion during the lithiation process[5,6]. Great efforts have been devoted to improving the rate performance and cycling stability of Li–S batteries, and two main strategies have been developed to confine the sulfur species in the cathode [3,7,8]. The first strategy is the physical encapsulation of elemental sulfur within carbonaceous nanomaterials[9–14] or inorganic matrices [15,16]. The ordered nanopores of polar and conductive inorganic hosts are essential for the homogenous distribution of elemental sulfur. However, the synthesis of inorganic matrices often involves complicated processes and strict conditions to achieve desired porosity, which is not favourable for large-scale application[17,18].

Alternatively, another strategy is covalently binding sulfur with organics to form organosulfur compounds[17–40]. When the circular S_8 molecule is heated to 159 °C, linear sulfur species with diradical chain ends are obtained via a ring opening reaction. After copolymerizing with organics containing specific functional groups, the organosulfur copolymers are prepared. By employing organosulfur copolymers as active cathode materials, the shuttle effect could be alleviated due to the strong covalent bonds between polymer chains and sulfur. The electrochemical properties of organics can be conveniently tailored by introducing diverse functional groups. Moreover, the abundant source of organics is

* Corresponding authors.
E-mail addresses: gckuang@csu.edu.cn (G.-C. Kuang), zhongjin@nju.edu.cn (Z. Jin).
[1] These authors contributed equally to this work.

https://doi.org/10.1016/j.cej.2021.130316
Received 24 February 2021; Received in revised form 17 April 2021; Accepted 8 May 2021
Available online 17 May 2021

conducive to the scalable synthesis of organosulfur copolymers. Currently, unsaturated hydrocarbon compounds[19,21,29,32,33] thiol-based[25,26,34–36], nitrile-based[28,37–39] and fluorinated polymers [24,30,31,40] are proposed as the skeletons for organosulfur copolymers. However, the relatively poor conducting nature of organosulfur copolymers seriously limits the rate capability, especially at a high sulfur content, and the inevitable shuttle effect still adversely affects the long-term cycling performance of Li–S batteries. Thus, it is highly desirable to explore new organosulfur copolymers with rational molecular structures and functional groups for high-performance Li–S batteries.

In this work, fluorinated quinone-derived organosulfur copolymers with high sulfur content were applied as active cathode materials for high-performance Li–S batteries. As shown in Fig. 1a, tetrafluorohydroquinone (TFHQ) was first self-polymerized into a crosslinked polymer (PTFHQ). Then, sulfurated-PTFHQ copolymer (PTFHQS) was prepared by copolymerizing elemental sulfur with the PTFHQ skeleton via a sulfur-ring opening reaction and subsequent nucleophilic aromatic substitution (S_NAr) reaction. As a control sample, tetrafluoro-p-benzoquinone (TFBQ) monomer was also copolymerized with elemental sulfur via a similar S_NAr reaction to obtain another organosulfur copolymer, TFBQS (Fig. 1b). The stable organosulfur copolymers of PTFHQS and TFBQS with high sulfur contents were facilely synthesized from lightweight PTFHQ and TFBQ organics, which could improve the battery energy density when considering the weight ratio of active sulfur species in the cathode. Abundant long-chain sulfur were covalently bonded to PTFHQ or TFBQ, and homogeneously distributed over the organosulfur copolymers at the molecular level. Due to the uniform distribution of sulfur species and the ample semi-ionic C–F bonds in the PTFHQS skeleton (Fig. 1c), the shuttle effect of polysulfides is effectively suppressed upon cycling. Moreover, the pre-polymerized PTFHQ skeleton exhibited improved electronic conductivity and facilitated Li-ion transportation, thus ensuring high rate capability and sulfur utilization.

2. Results and discussion

As shown in Fig. 1a, the TFHQ monomer was self-polymerized into the crosslinked polymer PTFHQ via a bimolecular nucleophilic substitution reaction between the deprotonated hydroxyl terminal and –F group of TFHQ. In view of the 1:2 stoichiometric ratio of –OH to –F, a

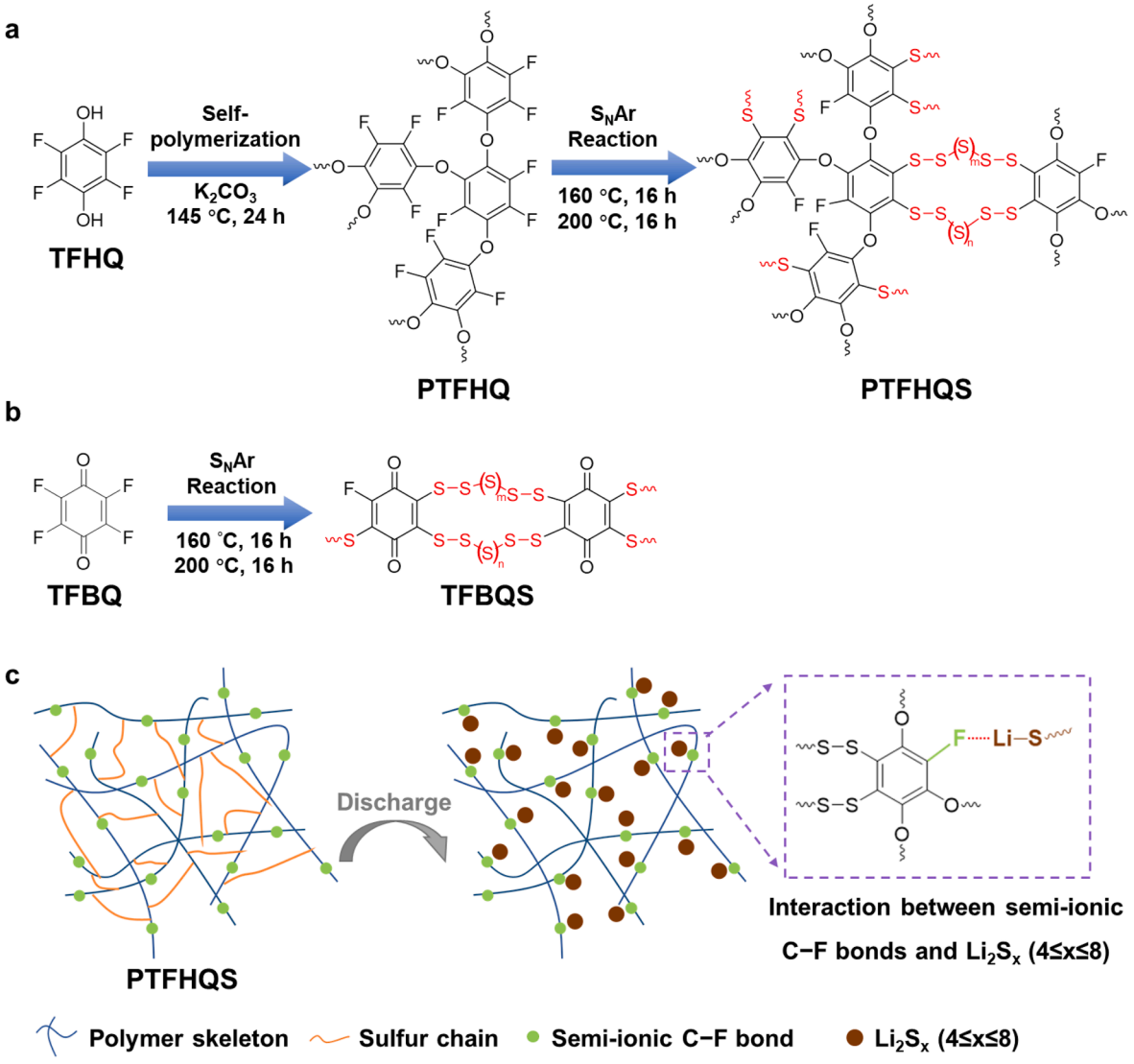

Fig. 1. Schematic diagram of the organosulfur copolymers as active cathode materials for Li–S batteries. (a) TFHQ is first self-polymerized into PTFHQ and then covalently linked to sulfur via S_NAr reaction. The as-obtained copolymer is referred to as PTFHQS. (b) Elemental sulfur is covalently linked to TFBQ through the S_NAr reaction, and the product is referred to as TFBQS. (c) Schematic illustration representing the Li···F interaction between Li_2S_x intermediates and the PTFHQS polymer skeleton with abundant semi-ionic C–F bonds.

portion of the –F group was substituted by –O– group in the self-polymerization process[41]. In the following S_NAr reaction, the nucleophilic intermediates obtained from the ring-opening of S_8 molecules reacted with the electron-deficient aromatic cores of PTFHQ under mild conditions (200 °C). According to elemental analysis, the sulfur content of the PTFHQS copolymer was measured to be 71 wt%. As a control sample, the TFBQS copolymer was obtained via a one-pot S_NAr reaction (Fig. 1b), in which the aromatic core of the TFBQ monomer directly reacted with the linear sulfur chains with diradical ends. According to elemental analysis, the sulfur content of the TFBQS copolymer was as high as 90 wt%. In regard to the weight ratio of active S species, the high sulfur contents in the organosulfur copolymers can greatly improve the energy density of Li–S batteries. Different from carbonaceous and polar inorganic host materials that physically encapsulate sulfur, the strategy of covalently crosslinking sulfur via C–S bonds in copolymers is not restricted by the size and volume of nanopores in the host matrices (Fig. 1c). Both PTFHQS and TFBQS copolymers can covalently attach sulfur chains to the molecular skeleton and have the merits of easy synthesis, high chemical stability and low cost.

Scanning electron microscopy (SEM) reveals that the as-prepared PTFHQS and TFBQS copolymers are micron-sized particles with irregular shapes (Figure S1). In these particles, sulfur is homogeneously distributed over the copolymers according to the energy-dispersive X-ray (EDX) spectroscopy analysis (Figure S2 and S3). Nitrogen adsorption/desorption isotherms and pore size distribution analysis reveal that the PTFHQ and TFBQ precursors are blocks with only a few nanopores (Figure S4), contributing to the high volumetric energy density of Li–S batteries. The molecular structures of PTFHQS and TFBQS copolymers were verified by attenuated total reflection-Fourier transform infrared (ATR-FTIR) spectroscopy. For the PTFHQS copolymer (Fig. 2a), the absorption peaks at 1053 and 740 cm^{-1} correspond to the C–O–C and C–F bonds, indicating the partial substitution of –F in the S_NAr reaction. In the ATR-FTIR spectrum of TFBQ (Fig. 2b), the strong peaks at 1321 and 736 cm^{-1} are attributed to C–F stretching and C–F bending, respectively. These peaks almost disappear in the spectrum of TFBQS copolymer, demonstrating the substitution of –F in the S_NAr reaction. Moreover, the C = O stretching band shifts from 1694 to 1634 cm^{-1}, revealing the polarity change of the aromatic cores by replacing –F with sulfur chains. Due to the weak intensity of the C–S absorption peak, no prominent peak is assigned to the formation of C–S bonds in the ATR-FTIR spectra of PTFHQS and TFBQS copolymers. In the Raman spectra of PTFHQS and TFBQS copolymers (Fig. 2c), three peaks at 151, 216, and 467 cm^{-1} are ascribed to the S–S stretching modes. For TFBQ monomer, the peak observed at 1700 cm^{-1} was assigned to C = C stretching[42]. However, this peak becomes less pronounced in the spectrum of organosulfur copolymer TFBQS, this is because the weight content of organic units in TFBQS (~10 wt%) after loading sulfur is much lower than that of TFBQ. The new formed C–S bonds and the thermostability of PTFHQS and TFBQS copolymers were evidenced by thermogravimetric analysis (TGA). The PTFHQS and TFBQS copolymers start to decompose at approximately 250 °C, corresponding to the pyrolysis and volatilization of sulfur species in the polymer backbones (Fig. 2d). Moreover, we find that the covalently tethered sulfur chains can improve the stability of TFBQS, since the TFBQ monomer begins to lose its weight at a considerably low temperature of approximately 60 °C. According to TGA results, the sulfur contents of PTFHQS and TFBQS are estimated to be ~ 71 wt% and ~ 90 wt%, respectively, which are in accordance with the results of the EDX and elemental analyses.

The chemical states of PTFHQS and TFBQS copolymers were examined by X-ray photoelectron spectroscopy (XPS). As shown in Fig. 3a, the XPS survey spectra confirm that the PTFHQS and TFBQS copolymers contain S, C, F and O species. The high-resolution XPS spectra of PTFHQS and TFBQS copolymers in the S 2p region (Fig. 3b) were deconvoluted into four peaks attributed to S–S (163.9 and 164.9 eV) and C–S bonds (163.1 and 163.8 eV)[25,34,43]. The high-resolution XPS spectrum of PTFHQ in the C 1 s region (Fig. 3c) shows three

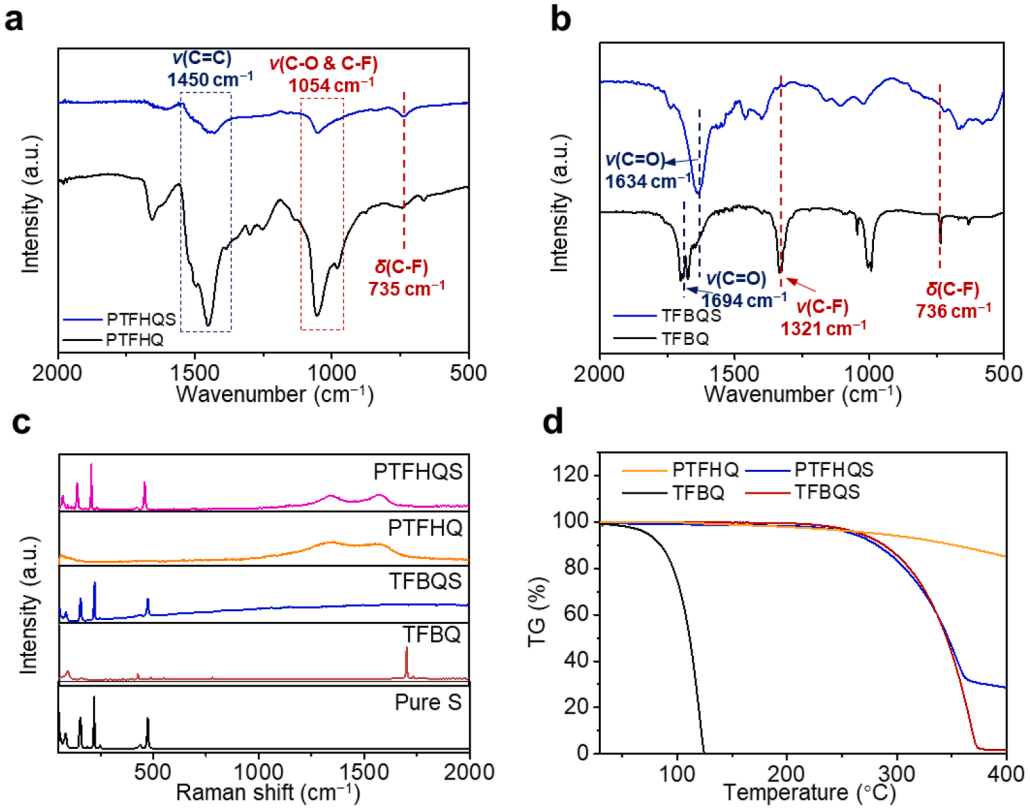

Fig. 2. Characterizations of PTFHQS, TFBQS copolymers and the corresponding precursors. (a) ATR-FTIR analysis of PTFHQS and PTFHQ. (b) ATR-FTIR analysis of TFBQS and TFBQ. (c) Raman spectra of PTFHQS, PTFHQ, TFBQS, TFBQ and elemental sulfur. (d) TGA curves of PTFHQS, PTFHQ, TFBQS and TFBQ.

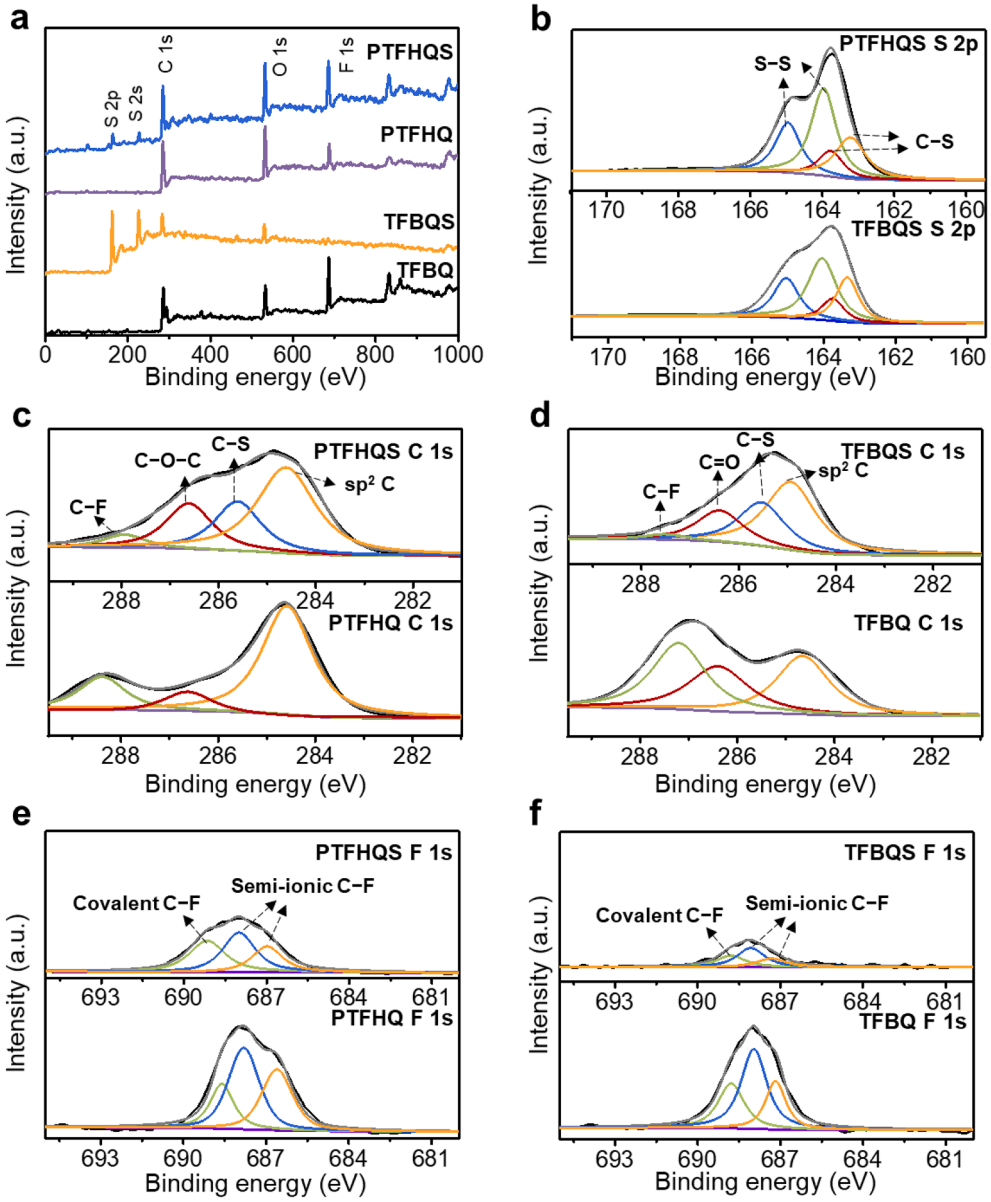

Fig. 3. XPS spectra of PTFHQS, TFBQS and the corresponding precursors. (a) XPS survey spectra of PTFHQS, PTFHQ, TFBQS and TFBQ. (b) High-resolution XPS spectra of PTFHQS and TFBQS in the S 2p region. High-resolution XPS spectra of (c) PTFHQS and PTFHQ and (d) TFBQS and TFBQ in the C 1 s region. High-resolution XPS spectra of (e) PTFHQS and PTFHQ, (f) TFBQS and TFBQ in the F 1 s region.

deconvoluted peaks at 284.6, 286.6 and 288.2 eV, which can be ascribed to sp^2 carbon, C–O–C, and C–F in fluorinated benzene [24,44]. Regarding to PTFHQS, the intensity of C–F peak decreases, and the new peak at 285.6 eV is ascribed to the C–S bonds[39,45,46], confirming the partial substitution of –F with sulfur chains. Similarly, three deconvoluted peaks of TFBQ at 284.6, 286.8, and 287.5 eV are designated to the sp^2 carbon, C = O, and semi-ionic C–F bonds(Fig. 3d). After the S_NAr reaction, the intensity of the C–F peak decreases, and a new peak at 285.4 eV ascribed to C–S bonds emerges. In the F 1 s band of PTFHQS, the deconvoluted peak at 689.1 eV is attributed to the covalent C–F bonds, and the deconvoluted peaks at 688.0 and 687.1 eV are corresponding to the F atoms semi-ionically bound to sp^2 carbon[30,47–50]. Compared with PTFHQ, the decreased intensities of the F 1 s band in PTFHQS also verify the S_NAr reaction between sulfur and aromatic fluoride (Fig. 3d and 3e).

To investigate the effect of reaction temperature to the structure and performance of organosulfur copolymer, another control sample of PTFHQS was synthesized by raising the S_NAr sulfurization temperature from 200 °C to 400 °C, namely PTFHQS-400. As shown in Figure S5a, for PTFHQS-400, the ATR-FTIR peak at 735 cm^{-1} corresponding to C–F bonds disappears, and the peaks attributed to phenyl group and C–O show slight decrease in intensity, implying the evident pyrolysis and removal of –F group at 400 °C[51]. The composition variation in PTFHQS-400 was also reflected by Raman spectroscopy (Figure S5b), in which the intensities of peaks at 1347 and 1540 cm^{-1} strengthen, indicating the formation of disordered and graphitic structures of carbonaceous material, respectively. To further identify the chemical states of PTFHQS-400, XPS analysis was also performed (Figure S6). In the high-resolution XPS at C 1 s region, the intensity ratio of peaks corresponding to sp^2 carbon (284.6 eV) and C–S (at 285.6 eV) significantly increases, confirming a greater extent of carbonization at 400 °C. According to the elemental analysis (Table S1), as the reaction temperature elevated from 200 to 400 °C, the contents of F and O decrease while the content of C increases. On the basis of the above characterizations, the changes of molecular structure at different S_NAr reaction temperatures were confirmed. The PTFHQS maintains an intact

polymetric structure at 200 °C, while it appears partial pyrolyzed and carbonized at 400 °C. Moreover, an increased number of C–F bonds decomposes at 400 °C, which may decrease the electrochemical performance of the cathode owing to the loss of polar and semi-ionic C–F bonds.

The electrochemical performance of PTFHQS and TFBQS copolymers was investigated as active cathode materials for Li–S batteries. The electrochemical behaviour of PTFHQS and TFBQS cathodes was investigated by cyclic voltammetry (CV). In Fig. 4a, two reduction peaks appear at ~ 2.2 and ~ 2.0 V, which are ascribed to the long-chain sulfur converting to intermediate polysulfides (Li_2S_x, $4 \leq x \leq 8$) and then further to Li_2S_2 or Li_2S, respectively. One broad oxidization peak at ~ 2.4 V is associated with the reverse conversion of short-chain sulfides to long-chain sulfur. The voltage polarization values, denoted as ΔE_1 and ΔE_2, are 0.14 and 0.35 V for the PTFHQS cathode, and 0.21 and 0.43 V for the TFBQS cathode, respectively. The smaller voltage polarization of PTFHQS cathode indicates the faster redox reaction kinetics. As shown in Figure S7a and Figure S7b, the electron-withdrawing –F substituent groups increase the reduction potential of carbonyl from 2.76 V vs. Li/Li^+ (as indicated by p-benzoquinone, pBQ) to 3.00 V vs. Li/Li^+ (for TFBQ monomer). When the applied potential is confined to the voltage range of conventional Li–S batteries (1.7–2.7 V vs. Li/Li^+), there are no redox peaks in the CV curves of TFBQ (Figure S7c). Moreover, the CV curve of TFBQS (Figure S7d) also shows no obvious redox peak of carbonyl redox reaction, indicating the minimal influence of carbonyl redox chemistry in the working potential of Li–S batteries. Electrochemical impedance spectroscopy (EIS) suggests that the PTFHQS and TFBQS cathodes exhibit low charge-transfer resistances (Figure S8), owing to the π-conjugated polymer unit and uniform distribution of sulfur species at a molecular level. Fig. 4b shows the rate performance of organosulfur copolymer cathodes at various current densities from 0.2 to 2.0C (1.0C = 1675 mA g^{-1}_{sulfur}). The PTFHQS cathode exhibits high discharge capacities of 893, 659, 443, and 307 mAh g^{-1}_{total} (calculated based on the total weight of organosulfur copolymer) and high Coulombic efficiencies of 97.7%, 98.4%, 99.3%, and 99.6% at 0.2, 0.5, 1.0, and 2.0C. The discharge capacities calculated based on the loading mass of sulfur are 1258, 930, 625, and 435 mAh g^{-1}_{sulfur} at 0.2, 0.5, 1.0, and 2.0C.The specific capacity of the PTFHQS cathode is restored to 854 mAh g^{-1}_{total} (1203 mAh g^{-1}_{total}) when the current density returns to 0.2C. The Li–S batteries assembled with the TFBQS cathodes exhibit specific discharge capacities of 802, 590, 396, and 212 mAh g^{-1}_{total} (891, 656, 440, and 236 mAh g^{-1}_{sulfur}) and Coulombic efficiencies of 88.7%, 92.5%, 95.5%, and 97.0% at 0.2, 0.5, 1.0, and 2.0C, respectively. Fig. 4c shows the representative galvanostatic charge/discharge profiles of the PTFHQS cathode, exhibiting two discharge plateaus and one slightly sloping charge plateau, which suggest that the PTFHQS cathode works well at high rates with highly reversible and thorough redox conversion of sulfur. In contrast, the TFBQS cathode at the high rate of 2.0C (Figure S9) exhibits large voltage polarization and sloping discharge plateau, signifying the sluggish redox kinetics and insufficient sulfur

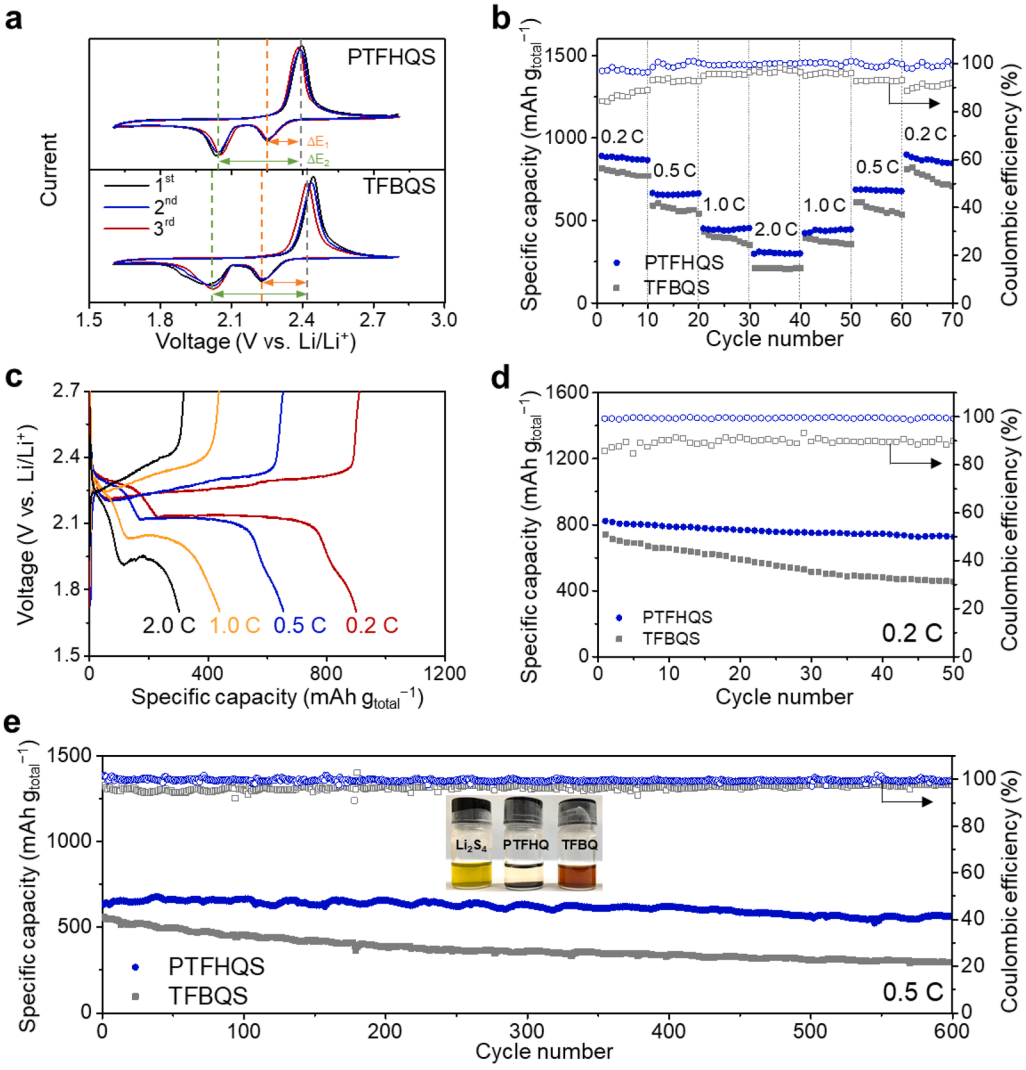

Fig. 4. Electrochemical performance of organosulfur copolymer cathodes for Li–S batteries. (a) CV curves of the PTFHQS and TFBQS cathodes at a scan rate of 0.1 mV s^{-1}. (b) Rate capability of the PTFHQS and TFBQS cathodes. (c) Representative galvanostatic charge/discharge voltage profiles of the PTFHQS cathode from 0.2C to 2.0C. (d) Cycling performance and Coulombic efficiencies of the PTFHQS and TFBQS cathodes at 0.2C. (e) Long-term cycling performance of the PTFHQS and TFBQS cathodes at 0.5C. The inset shows the comparison test of visual Li_2S_4 adsorption of PTFHQ and TFBQ monomer. The specific capacities are calculated according to the total mass of organosulfur copolymers in the cathodes. The areal mass loadings of sulfur on the cathodes are 1.0 mg_{sulfur} cm^{-2}.

utilization inferior to those of PTFHQS cathode.

The cycling performance of organosulfur copolymer cathodes at 0.2C are shown in Fig. 4d. The discharge capacity of PTFHQS cathode achieves an initial value of 823 mAh g^{-1}_{total} (1160 mAh g^{-1}_{sulfur}) and maintains at 726 mAh g^{-1}_{total} (1023 mAh g^{-1}_{sulfur}) after 50cycles. The capacity retention of PTFHQS cathode is 88.2% (0.23% capacity decay per cycle) with a high Coulombic efficiency of > 99% throughout the cycling process, indicating the effective alleviation of shuttle effect. The TFBQS cathode exhibits an initial discharge capacity of 741 mAh g^{-1}_{total} (823 mAh g^{-1}_{sulfur}) with a Coulombic efficiency of ~ 90% and keep at 456 mAh g^{-1}_{total} (507 mAh g^{-1}_{sulfur}) after 50cycles. Long-term cycling stabilities of PTFHQS and TFBQS cathodes were also tested at 0.5C (Fig. 4e). The PTFHQS cathode exhibits an initial discharge capacity of 643 mAh g^{-1}_{total} (905 mAh g^{-1}_{sulfur}) with a Coulombic efficiency above 99%. The discharge capacity remains stable and maintains at 564 mAh g^{-1}_{total} (794 mAh g^{-1}_{sulfur}) after 600cycles, which is accompanied by an average capacity decay of only 0.020% per cycle. In contrast, the TFBQS cathode shows an initial discharge capacity of 552 mAh g^{-1}_{total} (613 mAh g^{-1}_{sulfur}) and delivers 296 mAh g^{-1}_{total} (329 mAh g^{-1}_{sulfur}) after 600cycles (53.6% capacity retention, corresponding to an average capacity decay of 0.077% per cycle). As a control sample, PTFHQS-400 with less F content was also tested, as shown in Figure S10. The PTFHQS-400cathode delivers discharge capacities of 847, 724, 620 and 453 mAh g^{-1}_{total} (1283, 1097, 940 and 686 mAh g^{-1}_{sulfur}) at 0.2, 0.5, 1.0 and 2.0C, and exhibits average capacity decays of 0.65% at 0.2C and 0.29% at 0.5C per cycle, respectively. Owing to the increased conductivity and the decreased F content, the PTFHQS-400cathode exhibits better rate performance, but inferior cycling stability.These results indicate that the PTFHQS copolymer with prepolymerized skeleton and abundant C–F bonds can effectively confine sulfur species and alleviate the dissolution of polysulfides into electrolytes, thus resulting in remarkable cycling performance.

To further investigate the cycling stability of organosulfur copolymer cathodes, *ex-situ* UV–Vis absorption spectroscopy was conducted. As a control sample, a conventional S/C composite cathode was prepared by mixing S/C composite (with 80 wt% of elemental S, Figure S11), conductive carbon black and binder at a weight ratio of 70:20:10. The coin cells based on PTFHQS, TFBQS and conventional S/C cathodes were cycled for 30 times and disassembled at fully discharged state, and then immersed in dimethoxyethane/dioxolane solution (DME/DOL, 1:1 by volume) for 2 h. The DME/DOL solution soaked with the conventional S/C cathode shows absorption peaks at approximately 264, 282, 307, and 414 nm in the UV–Vis absorption spectrum (Figure S12), attributing to the dissolution of polysulfides in the electrolyte[52]. In contrast, the DME/DOL solution soaked with the PTFHQS cathode is almost colourless and shows much lower intensity of UV–Vis absorption peaks, suggesting the remarkable polysulfide trapping capability of PTFHQS cathode. The visual test results of Li_2S_4 adsorption are also shown in the inset of Fig. 4e. The Li_2S_4 solution was prepared by mixing S and Li_2S at a molar ratio of 3:1 in DME solvent. Then, 10 mg of PTFHQ or TFBQ was placed in 1.0 mL of DME solution with 0.005 M Li_2S_4. After mixing with PTFHQ particles, the colour of the Li_2S_4 solution rapidly changes from yellow to colourless, which is much lighter than the solution mixed with TFBQ. This suggests that the abundant semi-ionic C–F bonds with polar characteristics in the PTFHQ polymer have strong interactions with polysulfide species and thus can alleviate the shuttle effect.

Figure S13 shows the SEM images of the sulfur cathodes at fresh state and after charging/discharging for 100 cycles. The morphology of PTFHQS cathode was still maintained and no obvious change could be observed after long-term cycling. In contrast, for TFBQS cathode and S/C cathode, large and nonuniform blocks were observed on the surface after cycling. Furthermore, the morphology changes of Li anode surface before and after cycling were also observed through SEM (Figure S14). For the batteries assembled with PTFHQS cathode and TFBQS cathodes, the Li anodes show a dense and compact structure without inactive species. By contrast, the Li anode coupled with S/C cathode shows a rough and loose surface with appearance of micron-scale inactive species. These results verify that the shuttle effect was greatly weakened in Li–S batteries with PTFHQS cathodes. *Ex-situ* ATR-FTIR spectroscopy and XPS spectroscopy were carried out after long cycling test to verify the unchanged copolymer phase in PTFHQS cathode. As shown in Figure S15a, no discernible characteristic peaks changes are observed, indicating the stable molecular structure of PTFHQS. Moreover, the XPS C 1 s and S 2p profiles of the PTFHQS cathode after cycling clearly demonstrate the reversibility of charge/discharge processes (Figure S15b-f). Importantly, the deconvoluted C–S peaks at 285.6 eV indicate the robustness of C–S bonds within the copolymer framework.

In contrast to S/C composite, organosulfur copolymers with lower porosity contribute to increased compact density of sulfur cathodes (Figure S16) and superior volumetric energy density, which are crucial parameters for the practical application of Li–S batteries. The PTFHQS, TFBQS and S/C cathodes exhibit discharge capacities of 415,403 and 490 mAh g^{-1}_{total} (585, 448 and 612 mAh g^{-1}_{sulfur}) and volumetric capacities of 423, 419 and 292 mAh cm^{-3} at a rate of 1.0C, respectively. Furthermore, the low porosity of organosulfur cathodes also reduces the required volume of electrolyte, thus improving the gravimetric and volumetric capacities at cell level. Under lean electrolyte condition (10 μL mg^{-1}), the PTFHQS cathode exhibits normal electrochemical behavior, exhibiting discharge capacities of 764, 630, 467, and 241 mAh g^{-1}_{total} (1074, 887, 658, and 339 mAh g^{-1}_{sulfur}) at 0.2, 0.5, 1.0, and 2.0C, respectively (Figure S17). After charging/discharging at 0.5C and 2.0C, the PTFHQS cathodes deliver average capacity decays of 0.16% and 0.12% per cycle, respectively. These results indicate that the PTFHQS cathode features as a high-performance sulfur cathode, considering the high-rate capability, high gravimetric/volumetric capacity and cycling stability under high sulfur loading and lean electrolyte.

The reaction kinetics and Li-ion diffusivity of organosulfur copolymer cathodes with high sulfur loadings (2.0 mg_{sulfur} cm^{-2}) were evaluated by CV analysis at different scan rates. As shown in Fig. 5a, the oxidization peak of PTFHQS cathode at ~ 2.4 V is assigned to P1, and the reduction peaks at ~ 2.2 and ~ 2.0 V are assigned to P2 and P3, respectively. The peak currents of P1, P2 and P3 are linear with the square root of the scan rates, indicating a diffusion-controlled process. According to the Randles–Sevcik equation, the Li-ion diffusion coefficient (D^+_{Li}) can be calculated by the following equation[53,54]:

$$I = 2.69 \times 10^5 n^{3/2} A D^{1/2} v^{1/2} C_0 \quad (1)$$

where I is the peak current, n is the electron transfer number per reaction species, A is the electrode area, and C_0 is the Li-ion concentration in the cathode. Since n, A and C_0 are constant in the Li–S batteries, the absolute values of the fitting slopes show a positive correlation with Li-ion diffusivity. For the PTFHQS cathode, the slopes of P1, P2 and P3 are 11.58, –5.29, and –7.51 (Fig. 5b). For the TFBQS cathode, the sluggish conversion reaction of Li_2S_x ($4 \le x \le 8$) to Li_2S_2/Li_2S (P3, ~1.9 V) results in electrochemical polarization and insufficient sulfur utilization at high scan rates (Fig. 5c), and the slopes of P1 and P2 are 9.48 and 5.89, respectively (Fig. 5d). The conventional S/C cathode was also tested (Fig. 5e), in which the reduction peak corresponding to the conversion of Li_2S_x ($4 \le x \le 8$) to Li_2S_2/Li_2S is absent within the voltage window (1.7–2.7 V vs. Li/Li^+), and the slopes of P1 and P2 are 8.19 and 6.54, respectively (Fig. 5f). Clearly, the PTFHQS cathode exhibits much rapider Li-ion transport and better reaction kinetics than the TFBQS and conventional S/C cathodes. Moreover, the higher Li-ion diffusion coefficient of PTFHQS cathode also contributes to its superior polysulfide capture capability. For the TFBQS and conventional S/C cathodes, the larger amounts of Li_2S_x ($4 \le x \le 8$) intermediates dissolved into the electrolyte would lead to an increased viscosity and hamper Li-ion diffusion[55]. These results verify that the prepolymerized PTFHQ skeleton is beneficial to the homogeneous distribution of sulfur species and the effective alleviation of the shuttle effect, thus improving the active material utilization and cycling stability of Li–S batteries. The as-

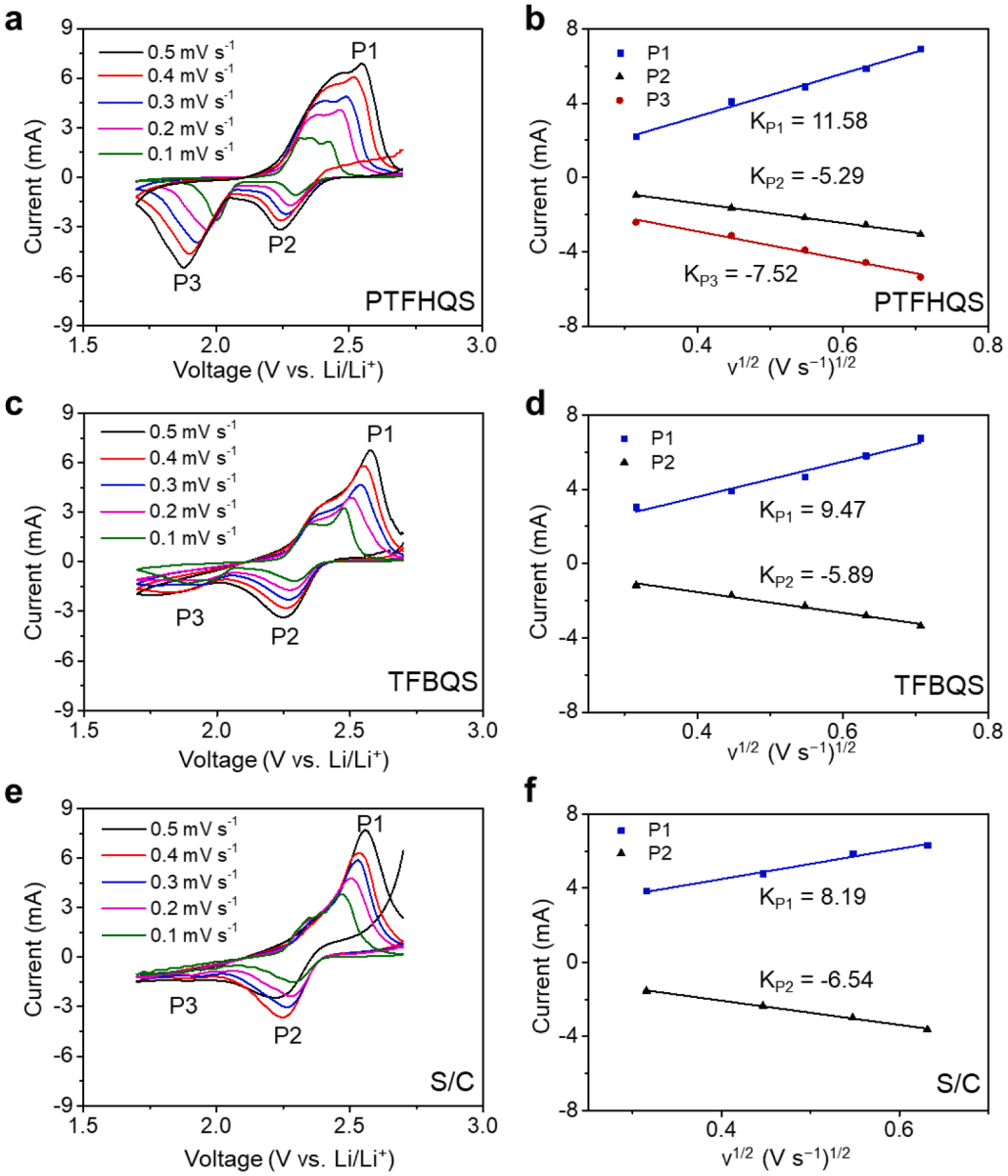

Fig. 5. CV curves of organosulfur copolymer and S/C cathodes at high sulfur loadings of 2.0 mg_{sulfur} cm^{-2}. (a, c, e) CV curves of (a) PTFHQS, (c) TFBQS and (e) conventional S/C cathodes at different scan rates. (b, d, f) The corresponding plots of the CV peak currents versus the square root of scan rates of (b) PTFHQS, (d) TFBQS and (f) conventional S/C cathodes.

prepared PTFHQS cathode shows a very competitive capacity and long-term cycling stability among the reported organosulfur cathodes (Table S2)[19,24–26,28–35,37–40].

For conventional Li–S batteries based on S/C cathode and ether-based electrolyte, high working temperature (>50 °C) will lead to more serious shuttle effect, resulting in worse cycle stability. Therefore, the heat endurance of Li–S batteries is significant for their practical application. According to our previous work, the flexible gel electrolyte based on elastic poly(vinylidene fluoride-hexafluoropropylene) (PVdF-HFP) matrix and 1-ethyl-3-methylimidazolium bis(trifluoromethylsulfonyl)imide (EMI-TFSI) ionic liquid (IL) additive shows excellent thermal stability due to the high degradation temperature of PVdF-HFP (>420 °C) and excellent thermal stability of IL (>400 °C) [56,57]. To evaluate the performance stability of PTFHQS cathode at high temperatures, Li–S batteries with specific sulfur-containing cathode, gel electrolyte, and Li foil anode were assembled. Fig. 6a shows the performances of PTFHQS, TFBQS, and S/C cathodes under various temperatures raised from 20 °C to 80 °C. Generally, the specific capacities of the cells were improved at higher temperatures due to faster kinetics and more complete conversion of active materials. When the working temperature was raised from 20 °C to 80 °C, the PTFHQS cathode exhibited the most stable capacities (561 mAh g^{-1}_{total},789 mAh g^{-1}_{sulfur}) at 1.0C and the highest Coulombic efficiencies (98.1%) among these samples (Fig. 6a). At 80 °C, the discharge capacities of PTFHQS cathodes are 938, 724, 548, and 427 mAh g^{-1}_{total} (1321, 1020, 772, and 601 mAh g^{-1}_{sulfur}) with Coulombic efficiencies of 96.5%, 97.2%, 98.8%, and 99.4% at 0.2, 0.5, 1.0, and 2.0C, suggesting remarkable rate capability at high temperature (Fig. 6b, 6c). Fig. 6d shows the cycling stability test of the PTFHQS cathode with large sulfur loading of 2 mg cm^{-2} at room temperature (20 °C) and extremely high temperature (80 °C). The discharge capacities reached 89% and 78% of the initial capacity after 100cycles at 2.0C, respectively, suggesting the good thermal endurance and highly stable cyclability. The results show that the PTFHQS cathode can effectively restrict the dissolution of lithium polysulfides into the electrolyte and maintain long-term stability at raised temperatures.

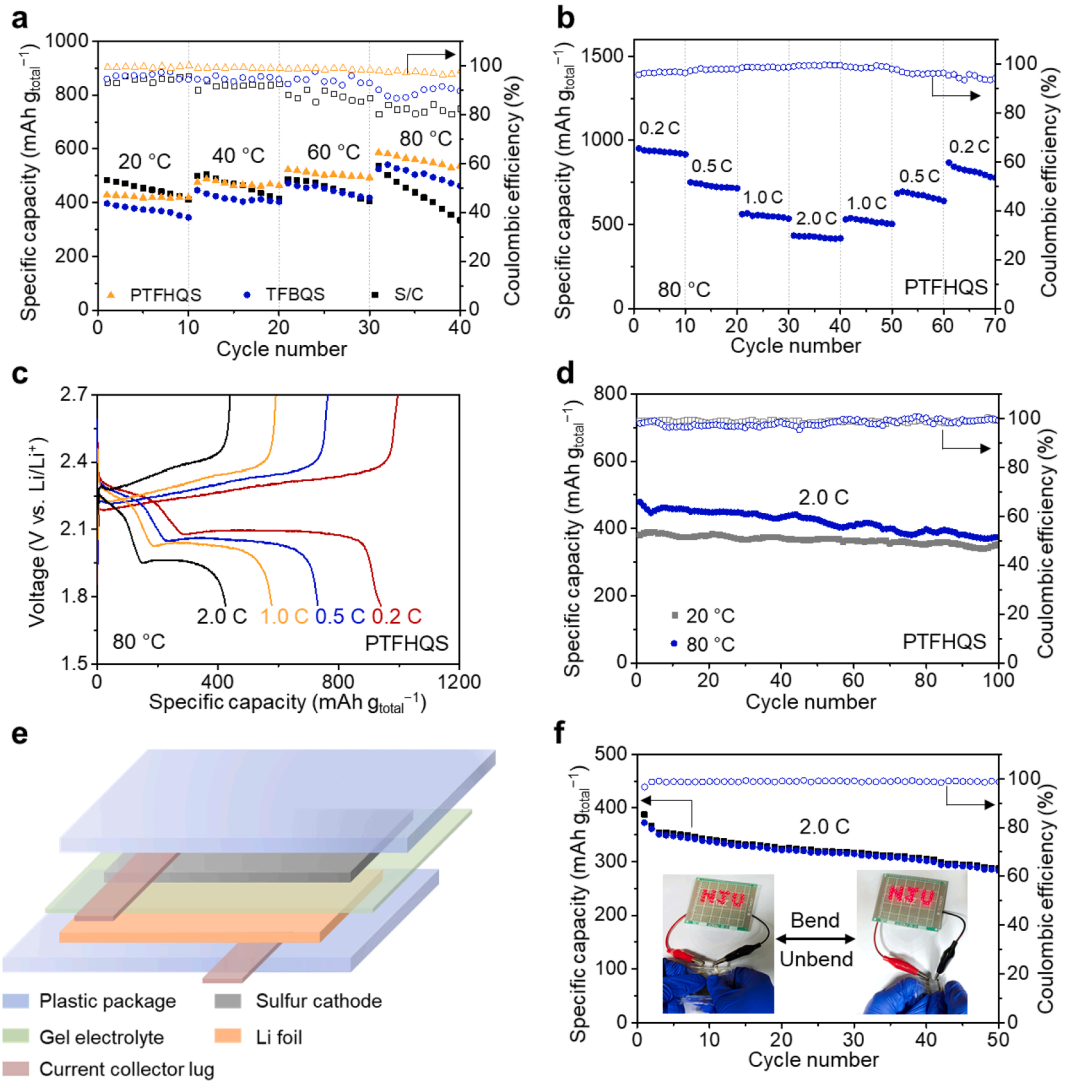

Fig. 6. Thermal stability and flexibility of the Li–S batteries based on PTFHQS cathodes at high sulfur loadings of 2.0 mg$_{sulfur}$ cm^{-2}. (a) Specific capacities and Coulombic efficiencies of Li–S batteries assembled with PTFHQS, TFBQS, and conversional S/C cathodes tested at various temperatures from 20 °C to 80 °C at 1.0C. (b) Rate performance and (c) corresponding charge/discharge curves of the PTFHQS cathode at various current densities from 0.2 to 2.0C at the elevated working temperature of 80 °C. (d) Long-term cycling performance of PTFHQS cathode under 20 °C and 80 °C at 2.0C. (e) Schematic configuration of a soft-packed Li–S battery assembled with the PTFHQS cathode, gel electrolyte, and Li foil anode. (f) Cycling stability of a flexible soft-packed Li–S battery assembled with the PTFHQS cathode, gel electrolyte, and Li foil anode tested at 2.0C under continuous bending/unbending operation. The insert shows the flexible soft-packed Li–S battery based on PTFHQS cathode (size: 3 cm × 2 cm) lighting up a lamp panel of 25 LEDs during continuous bending-unbending cycles.

To verify the good flexibility and stability of PTFHQS polymer, soft-packed Li–S batteries were assembled according to the structural configuration depicted in Fig. 6e. In a typical procedure, the gel electrolyte was sandwiched between the PTFHQS cathode (3 × 2 cm^2) and Li foil anode and then sealed with plastic package. As shown in the insert of Fig. 6f, the soft-packed Li–S battery was used to power up a lamp panel with 25 light emitting diodes (LEDs) during continuous bending-unbending processes. The brightness of the LEDs exhibited no visual disparity when the soft-packed battery was continuously bended and recovered. Fig. 6f shows the performance stability test of the soft-packed Li–S battery under continuous bending/unbending operation. The initial discharge capacity is 373 mAh g_{total}^{-1} (526 mAh g_{sulfur}^{-1}) under 2.0C, and remained 288 mAh g_{total}^{-1} (406 mAh g_{sulfur}^{-1}) after 50cycles (with a capacity retention of 77.2%). Figure S18 indicates that the PTFHQS cathode maintains good integrity after cyclic bending-unbending tests due to its compact structure and strong adhesive force. By contrast, conventional S/C composite cathode shows severe detaching and shedding phenomena during deformation tests, owing to the bad adhesive property of S/C composites consisting of high-surface-area and low-density carbon black[58]. These results suggest the high robustness and stable electrochemical performance of the flexible organosulfur PTFHQS copolymer cathodes under dynamic conditions.

3. Conclusion

In summary, fluorinated quinone-derived organosulfur copolymer PTFHQS with a high sulfur content has been successfully synthesized and utilized as a high-performance cathode material in Li–S batteries. Linear sulfur chains were covalently attached to the predesigned PTFHQ polymer skeleton by partially substituting –F with –S$_x$– via a nucleophilic aromatic substitution (S$_N$Ar) reaction. The homogeneous distribution of sulfur chains in the PTFHQS copolymer at a molecular level endowed excellent Li-ion diffusivity, sufficient capacity utilization and fast redox kinetics. Compared with the TFBQS organosulfur copolymer, the abundant semi-ionic C–F bonds with polar characteristics in PTFHQS are beneficial for suppressing the shuttle effect during cycling even at a

high temperature of 80 °C. The PTFHQS cathode with a 71 wt% sulfur content delivers a high discharge capacity of 643 mAh g^{-1}_{total} with Coulombic efficiencies above 99%, and also maintains 87% of its initial capacity after 600 cycles. Moreover, the Li–S batteries based on PTFHQS cathode show remarkable thermal resistance and flexibility. We hope this work may provide new insights and inspirations for designing advanced organosulfur copolymers with well-designed molecular structures for achieving high-performance Li–S batteries.

4. Methods

Chemicals. All commercially available reagents and solvents were used as received without further purification.

Synthesis of PTFHQ. In a typical procedure, tetrafluorohydroquinone (TFHQ, 500 mg, 2.74 mmol) was dispersed in DMF (20 mL) under vigorous stirring in a round-bottom flask. Subsequently, the mixture was heated to 80 °C, and K_2CO_3 (250 mg, 1.81 mmol) was added to the above mixture. Then, the solution was heated to 145 °C and stirred for 24 h. After naturally cooling to room temperature, deionized water (DIW, 200 mL) was added, and the mixture was stirred for 4 h. The obtained precipitate product was filtered and washed thoroughly with DIW (500 mL) and acetone (50 mL) until a clear filtrate was observed. The resulting powder was dried at 120 °C under vacuum overnight and denoted as PTFHQ (440 mg, yield ratio 88%).

Synthesis of PTFHQS and PTFHQS-400. Poly(tetrafluorohydroquinone) (PTFHQ, 30 mg) and elemental sulfur (90 mg, 2.81 mmol) were added into a glass tube (10 mL, the outer diameter was 10 mm, and the inner diameter was 8 mm). The tube was degassed and sealed by an open flame. The mixture was heated to 160 °C and maintained at 160 °C for 16 h; then the mixture was further heated to 200 °C and maintained at 200 °C for 16 h. After cooling to room temperature, the obtained product was denoted as PTFHQS (112 mg, yield ratio 93%). The control sample of PTFHQS-400 was synthesized at varying reaction temperature. Briefly, the PTFHQ/S mixture was first heated at 160 °C for 16 h and then increased to 400 °C for another 16 h. The yield ratio of PTFHQS-400 was 80%.

Synthesis of TFBQS. Tetrafluoro-p-benzoquinone (TFBQ, 30 mg, 0.17 mmol) and elemental sulfur (90 mg, 2.81 mmol) were added into a glass tube (10 mL, the outer diameter was 10 mm, and the inner diameter was 8 mm). The tube was degassed and sealed by an open flame. The mixture was heated to 160 °C and maintained at 160 °C for 16 h; then the mixture was further heated to 200 °C and maintained at 200 °C for 16 h. After cooling to room temperature, the obtained product was a brown powder and denoted as TFBQS (83 mg, yield ratio 69%).

Preparation of conventional S/C composite. The S/C composite was obtained via a melt-diffusion method. Briefly, the mixture of elemental S and Ketjen black carbon nanoparticles (with a mass ratio of 8:2) was ball-milled for 30 min and then heated at 155 °C for 16 h in a Teflon-lined 50-mL autoclave.

Fabrication of the gel electrolyte. The gel electrolyte was prepared via a modified method in our previous work[56,57]. Briefly, PVdF-HFP (1000 mg) and 1-ethyl-3-methylimidazolium bis(trifluoromethylsulfonyl)imide (EMI-TFSI, 400 mg) were added to anhydrous acetone (10 mL) and vigorously stirred for 4 h. The resultant solution was poured into a flat polytetrafluoroethylene (PTFE) mould (size: 4 × 6 cm^2) and dried at 4 °C overnight to form a uniform IL-PVdF-HFP membrane. The IL-PVdF-HFP membrane was then soaked in the LiTFSI solution for 20 min to form the gel electrolyte.

Material characterizations. Elemental analysis was carried out using an Elementar Vario MICRO cube to characterize the quantitative sulfur content in copolymers. ATR-FTIR spectroscopy was conducted with a Thermo Scientifc NICOLET iS10 instrument. Raman spectroscopy was performed on a Horiba JY Raman spectrometer using a 633 nm laser source. Thermogravimetric analysis (TGA) was conducted in a N_2 flow on a thermogravimetric/differential thermal analyser (Netzsch, STA 449C) at a heating rate of 10 °C min^{-1}. Scanning electron microscopy (SEM) was conducted with an FEI Nova NanoSEM 450 equipped with an attached EDX apparatus (Bruker Quantax-200). Nitrogen adsorption–desorption isotherms were measured through Brunauer–Emmett–Teller (BET) model at 77 K on a Quantachrome Autosorb-IQ-2C-TCD-VP instrument. X-ray photoelectron spectroscopy (XPS) measurements were conducted with a PHI-5000 Versa Probe X-ray photoelectron spectrometer using an Al Kα radiation source. UV–Vis absorption spectra were collected with a Shimadzu UV-2600 spectrometer.

Electrochemical measurements. The organosulfur copolymer cathodes were prepared by mixing the organosulfur copolymer, acetylene black and binder (polyvinylidene fluoride, PVDF) in N-methylpyrrolidinone (NMP) solvent at a weight ratio of 70:20:10. The mixture was stirred for 24 h, spread on a carbon-coated aluminium foil with a doctor blade, and then dried in a vacuum oven at 60 °C overnight to remove the solvent. Li–S coin cells (CR2032 type) were assembled in an argon-filled glove box with the above cathodes, lithium metal foil as anodes and polypropylene separators (Celgard 2400). A solution of 1.0 M bis(trifluoromethane)sulfonamide lithium (LiTFSI) dissolved in a mixed solvent of 1,2-dimethoxyethane (DME) and 1,3-dioxolane (DOL) at a 1:1 vol ratio containing $LiNO_3$ (1 wt%) was used as the electrolyte, and 15 μL mg^{-1}_{sulfur} of the electrolyte was used in the coin cells unless stated otherwise. Cyclic voltammetry (CV) curves and electrochemical impedance spectra (EIS) were collected on a Chenhua CHI-760e electrochemical workstation. EIS analysis was carried out from 100 kHz to 0.01 Hz at an amplitude of 5 mV. The galvanostatic cycling performances of Li–S batteries were measured on a LAND CT2001A analyser at different current densities within a potential window of 1.7–2.7 V vs Li/Li^+. The specific capacities were calculated based on the loading weight of organosulfur copolymers.

Declaration of Competing Interest

The authors declare that they have no known competing financial interests or personal relationships that could have appeared to influence the work reported in this paper.

Acknowledgements

This work was financially supported by the National Key Research and Development Program of China (2017YFA0208200), the Fundamental Research Funds for the Central Universities of China (0205-14380219, 0205-14913212), the Natural Science Foundation of China (22022505, 21872069), the Natural Science Foundation of Jiangsu Province (BK20180008), the Natural Science Foundation of Hunan Province (2020JJ4679) of China, and the Shenzhen Fundamental Research Program of Science, Technology and Innovation Commission of Shenzhen Municipality (JCYJ20180307155007589).

Appendix A. Supplementary data

Supplementary data to this article can be found online at https://doi.org/10.1016/j.cej.2021.130316.

References

[1] X. Ji, K.T. Lee, L.F. Nazar, A highly ordered nanostructured carbon–sulphur cathode for lithium–sulphur batteries, Nat. Mater. 8 (2009) 500–506.
[2] P.G. Bruce, S.A. Freunberger, L.J. Hardwick, J.M. Tarascon, Li–O_2 and Li–S batteries with high energy storage, Nat. Mater. 11 (2012) 19–29.
[3] S. Evers, L.F. Nazar, New approaches for high energy density lithium–sulfur battery cathodes, Acc. Chem. Res. 46 (2013) 1135–1143.
[4] J. Ma, Y. Li, N.S. Grundish, J.B. Goodenough, Y. Chen, L. Guo, Z. Peng, X. Qi, F. Yang, L. Qie, C.-A. Wang, B. Huang, Z. Huang, L. Chen, D. Su, G. Wang, X. Peng, Z. Chen, J. Yang, S. He, X. Zhang, H. Yu, C. Fu, M. Jiang, W. Deng, C.-F. Sun, Q. Pan, Y. Tang, X. Li, X. Ji, F. Wan, Z. Niu, F. Lian, C. Wang, G.G. Wallace, M. Fan, Q. Meng, S. Xin, Y.-G. Guo, L.-J. Wan, The 2021 Battery Technology Roadmap, J. Phys. D: Appl. Phys. 54 (2021), 183001.

[5] R. Fang, S. Zhao, Z. Sun, W. Wang, H.M. Cheng, F. Li, More reliable lithium-sulfur batteries: status, solutions and prospects, Adv. Mater. 29 (2017) 1606823.

[6] L. Kong, B.Q. Li, H.J. Peng, R. Zhang, J. Xie, J.Q. Huang, Q. Zhang, Porphyrin-derived graphene-based nanosheets enabling strong polysulfide chemisorption and rapid kinetics in lithium-sulfur batteries, Adv. Energy Mater. 20 (2018) 1800849.

[7] W. Li, J. Liu, D. Zhao, Mesoporous materials for energy conversion and storage devices, Nat. Rev. Mater. 1 (2016) 16023.

[8] Z. Li, Y. Huang, L. Yuan, Z. Hao, Y. Huang, Status and prospects in sulfur–carbon composites as cathode materials for rechargeable lithium–sulfur batteries, Carbon 92 (2015) 41–63, https://doi.org/10.1016/j.carbon.2015.03.008.

[9] T. Chen, B. Cheng, G. Zhu, R. Chen, Y. Hu, L. Ma, H. Lv, Y. Wang, J. Liang, Z. Tie, Z. Jin, J. Liu, Highly efficient retention of polysulfides in "sea urchin"-like carbon nanotube/nanopolyhedra superstructures as cathode material for ultralong-life lithium–sulfur batteries, Nano Lett. 17 (2017) 437–444.

[10] R. Fang, G. Li, S. Zhao, L. Yin, K. Du, P. Hou, S. Wang, H.-M. Cheng, C. Liu, F. Li, Single-wall carbon nanotube network enabled ultrahigh sulfur-content electrodes for high-performance lithium-sulfur batteries, Nano Energy 42 (2017) 205–214, https://doi.org/10.1016/j.nanoen.2017.10.053.

[11] L. Ji, M. Rao, H. Zheng, L. Zhang, Y. Li, W. Duan, J. Guo, E.J. Cairns, Y. Zhang, Graphene Oxide as a sulfur immobilizer in high performance lithium/sulfur cells, J. Am. Chem. Soc. 133 (2011) 18522–18525.

[12] C. Zu, A. Manthiram, Hydroxylated graphene-sulfur nano composites for high-rate lithium-sulfur batteries, Adv. Energy Mater. 3 (2013) 1008–1012.

[13] H. Peng, J.Q. Huang, M.Q. Zhao, Q. Zhang, X.B. Cheng, X.Y. Liu, W.Z. Qian, F. Wei, Nanoarchitectured graphene/CNT@porous carbon with extraordinary electrical conductivity and interconnected micro/mesopores for lithium-sulfur batteries, Adv. Funct. Mater. 24 (2014) 2772–2781.

[14] Q. Sun, B. He, X.-Q. Zhang, A.-H. Lu, Engineering of Hollow Core–Shell Interlinked Carbon Spheres for Highly Stable Lithium–Sulfur Batteries, ACS Nano 9 (8) (2015) 8504–8513, https://doi.org/10.1021/acsnano.5b03488.

[15] L. Ma, R. Chen, G. Zhu, Y.i. Hu, Y. Wang, T. Chen, J. Liu, Z. Jin, Cerium Oxide Nanocrystal Embedded Bimodal Micromesoporous Nitrogen-Rich Carbon Nanospheres as Effective Sulfur Host for Lithium–Sulfur Batteries, ACS Nano 11 (7) (2017) 7274–7283, https://doi.org/10.1021/acsnano.7b03227.s001.

[16] X. Liu, J.Q. Huang, Q. Zhang, L. Mai, Nanostructured metal oxides and sulfides for lithium–sulfur batteries, Adv. Mater. 29 (2017) 1601759.

[17] J. Liu, M. Wang, N.a. Xu, T. Qian, C. Yan, Progress and perspective of organosulfur polymers as cathode materials for advanced lithium-sulfur batteries, Energy Storage Materials 15 (2018) 53–64, https://doi.org/10.1016/j.ensm.2018.03.017.

[18] X. Zhang, K. Chen, Z. Sun, G. Hu, R. Xiao, H.M. Cheng, F. Li, Structure-related electrochemical performance of organosulfur compounds for lithium–sulfur batteries, Energ. Environ. Sci. 13 (2020) 1076.

[19] B. Oschmann, J. Park, C. Kim, K. Char, Y.E. Sung, R. Zentel, Copolymerization of polythiophene and sulfur to improve the electrochemical performance in lithium–sulfur batteries, Chem. Mater. 27 (2015) 7011–7017.

[20] S. Park, S.J. Kim, Y.E. Sung, K. Char, J.G. Son, Short-chain polyselenosulfide copolymers as cathode materials for lithium–sulfur batteries, ACS Appl. Mater. Inter. 11 (2019) 45785–45795.

[21] X. Liu, S. Wang, A. Wang, J. Chen, Z. Wang, Q. Zeng, W. Liu, Z. Li, L. Zhang, A new conjugated porous polymer with covalently linked polysulfide as cathode material for high-rate capacity and high coulombic efficiency lithium–sulfur batteries, J. Phys. Chem. C. 123 (2019) 21327–21335.

[22] Y. Tsao, Z. Chen, S.R. Gagné, Q. Zhang, H. Yao, S. Chen, G. Zhou, C. Zu, Y. Cui, Z. Bao, Enhanced cycling stability of sulfur electrodes through effective binding of pyridine-functionalized polymer, ACS Energy Lett. 2 (2017) 2454–2462.

[23] S. Huang, R. Guan, S. Wang, M. Xiao, D. Han, L. Sun, Y. Meng, Polymers for high performance Li-S batteries: material selection and structure design, Prog. Polym. Sci. 89 (2019) 19–60.

[24] S.H. Je, H.J. Kim, J. Kim, J.W. Choi, A. Coskun, Perfluoroaryl-elemental sulfur S_NAr chemistry in covalent triazine frameworks with high sulfur contents for lithium–sulfur batteries, Adv. Funct. Mater. 27 (2017) 1703947.

[25] H. Kim, J. Lee, H. Ahn, O. Kim, M.J. Park, Synthesis of three-dimensionally interconnected sulfur-rich polymers for cathode materials of high-rate lithium–sulfur batteries, Nat. Commun. 6 (2015) 7278–7287.

[26] N. Xu, T. Qian, X. Liu, J. Liu, Y. Chen, C. Yan, Greatly suppressed shuttle effect for improved lithium sulfur battery performance through short chain intermediates, Nano Lett. 17 (2017) 538–543.

[27] M. Wang, W. Wang, A. Wang, K. Yuan, L. Miao, X. Zhang, Y. Huang, Z. Yu, J. Qiu, A multi-core–shell structured composite cathode material with a conductive polymer network for Li–S batteries, Chem. Commun. 49 (2013) 10263–10265.

[28] S. Wei, L. Ma, K.E. Hendrickson, Z. Tu, L.A. Archer, Metal–sulfur battery cathodes based on PAN–sulfur composites, J. Am. Chem. Soc. 137 (2015) 12143–12152.

[29] Z. Sun, M. Xiao, S. Wang, D. Han, S. Song, G. Chen, Y. Meng, Sulfur-rich polymeric materials with semi-interpenetrating network structure as a novel lithium–sulfur cathode, J. Mater. Chem. A 2 (24) (2014) 9280, https://doi.org/10.1039/c4ta00779d.

[30] D.G. Wang, N. Li, Y. Hu, S. Wan, M. Song, G. Yu, Y. Jin, W. Wei, K. Han, G. C. Kuang, W. Zhang, Highly fluoro-substituted covalent organic framework and its application in lithium–sulfur batteries, ACS Appl. Mater. Inter. 10 (2018) 42233–42240.

[31] J. Kim, A. Elabd, S.Y. Chung, A. Coskun, J.W. Choi, Covalent triazine frameworks incorporating charged polypyrrole channels for high-performance lithium–sulfur batteries, Chem. Mater. 32 (2020) 4185–4193.

[32] W.J. Chung, J.J. Griebel, E.T. Kim, H. Yoon, A.G. Simmonds, H.J. Ji, P.T. Dirlam, R. S. Glass, J.J. Wie, N.A. Nguyen, B.W. Guralnick, J. Park, A. Somogyi, P. Theato, M. E. Mackay, Y.-E. Sung, K. Char, J. Pyun, The use of elemental sulfur as an alternative feedstock for polymeric materials, Nat. Chem. 5 (2013) 518–524.

[33] J. Park, E.T. Kim, C. Kim, J. Pyun, H.-S. Jang, J. Shin, J.W. Choi, K. Char, Y.-E. Sung, The importance of confined sulfur nanodomains and adjoining electron conductive pathways in subreaction regimes of Li-S batteries, Adv. Energy Mater. 7 (2017) 1700074.

[34] S.H. Je, T.H. Hwang, S.N. Talapaneni, O. Buyukcakir, H.J. Kim, J.-S. Yu, S.-G. Woo, M.C. Jang, B.K. Son, A. Coskun, J.W. Choi, Rational sulfur cathode design for lithium–sulfur batteries: sulfur-embedded benzoxazine polymers, ACS Energy Lett. 1 (2016) 566–572.

[35] S. Zeng, L. Li, L. Xie, D. Zhao, N. Wang, S. Chen, Conducting Polymers Crosslinked with Sulfur as Cathode Materials for High-Rate, Ultralong-Life Lithium-Sulfur Batteries, ChemSusChem 10 (17) (2017) 3378–3386, https://doi.org/10.1002/cssc.201700913.

[36] A. Bhargav, M.E. Bell, J. Karty, Y.i. Cui, Y. Fu, A Class of Organopolysulfides As Liquid Cathode Materials for High-Energy-Density Lithium Batteries, ACS Appl. Mater. Interfaces 10 (25) (2018) 21084–21090, https://doi.org/10.1021/acsami.8b06803.s001.

[37] J. Wang, J. Yang, C. Wan, K. Du, J. Xie, N. Xu, Sulfur composite cathode materials for rechargeable lithium batteries, Adv. Funct. Mater. 13 (2003) 487–492.

[38] S.N. Talapaneni, T.H. Hwang, S.H. Je, O. Buyukcakir, J.W. Choi, A. Coskun, Elemental-sulfur-mediated facile synthesis of a covalent triazine framework for high-performance lithium–sulfur batteries, Angew. Chem. Int. Edit. 55 (2016) 3106–3111.

[39] X. Chen, L. Peng, L. Wang, J. Yang, Z. Hao, J. Xiang, K. Yuan, Y. Huang, B. Shan, L. Yuan, J. Xie, Ether-compatible sulfurized polyacrylonitrile cathode with excellent performance enabled by fast kinetics via selenium doping, Nat. Commun. 10 (2019) 1021.

[40] H. Shin, D. Kim, H.J. Kim, J. Kim, K. Char, C.T. Yavuz, J.W. Choi, Fluorinated covalent organic polymers for high performance sulfur cathodes in lithium–sulfur batteries, Chem. Mater. 31 (2019) 7910–7921.

[41] J. Byun, H.A. Patel, D. Thirion, C.T. Yavuz, Charge-specific size-dependent separation of water-soluble organic molecules by fluorinated nanoporous networks, Nat. Commun. 7 (2016) 13377.

[42] A. Girlando, C. Pecile, Vibrational spectra of fluoranil. (2, 3, 5, 6-Tetrafluoro-p-benzoquinone), J. Chem. Soc., Faraday Trans. 2 71 (1975) 689, https://doi.org/10.1039/f29757100689.

[43] X.-G. Yu, J.-Y. Xie, J. Yang, H.-J. Huang, K. Wang, Z.-S. Wen, Lithium storage in conductive sulfur-containing polymers, J. Electroanal. Chem. 573 (2004) 121–128.

[44] F. Li, J. He, J. Liu, M. Wu, Y. Hou, H. Wang, S. Qi, Q. Liu, J. Hu, J. Ma, Gradient Solid Electrolyte Interphase and Lithium-Ion Solvation Regulated by Bisfluoroacetamide for Stable Lithium Metal Batteries, Angew. Chem. Int. Edit. 60 (2021) 6600–6608.

[45] J. Zhou, T. Qian, N. Xu, M. Wang, X. Ni, X. Liu, X. Shen, C. Yan, Selenium-doped cathodes for lithium–organosulfur batteries with greatly improved volumetric capacity and coulombic efficiency, Adv. Mater. 29 (2017) 1701294.

[46] L. Duan, W. Kong, W. Yan, C.-H. Li, Z. Jin, J.-L. Zuo, Improving the capacity and cycling-stability of lithium–sulfur batteries by self-healing binders containing dynamic disulfide bonds, Sustain. Energy Fuels 4 (2020) 2760–2767.

[47] S. Qi, H. Wang, J. He, J. Liu, C. Cui, M. Wu, F. Li, Y. Feng, J. Ma, Electrolytes Enriched by Potassium Perfluorinated Sulfonates for Lithium Metal Batteries, Sci. Bull. 66 (2021) 685–693.

[48] Z. Li, W. Niu, Z. Yang, N. Zaman, W. Samarakoon, M. Wang, A. Kara, M. Lucero, M. V. Vyas, H. Cao, H. Zhou, G.E. Sterbinsky, Z. Feng, Y. Du, Y. Yang, Stabilizing atomic Pt with trapped interstitial F in alloyed PtCo nanosheets for high-performance zinc-air batteries, Energy Environ. Sci. 13 (2020) 884–895.

[49] L. Ju, G. Wang, K. Liang, M. Wang, G.E. Sterbinsky, Z. Feng, Y. Yang, Significantly improved cyclability of conversion-type transition metal oxyfluoride cathodes by homologous passivation layer reconstruction, Adv. Energy Mater. 10 (2020) 1903333.

[50] F. Xu, S. Yang, G. Jiang, Q. Ye, B. Wei, H. Wang, Fluorinated, sulfur-rich, covalent triazine frameworks for enhanced confinement of polysulfides in lithium–sulfur batteries, ACS Appl. Mater. Inter. 9 (2017) 37731–37738.

[51] M. L. O'shea, C. Morterra, M. J. D. Low, Spectroscopic studies of carbons. XVII. Pyrolysis of polyvinylidene fluoride. Mater. Chem. Phys. 1990, 26, 195–205.

[52] T. Chen, Z. Zhang, B. Cheng, R. Chen, Y. Hu, L. Ma, G. Zhu, J. Liu, Z. Jin, Self-templated formation of interlaced carbon nanotubes threaded hollow Co_3S_4 nanoboxes for high-rate and heat-resistant lithium-sulfur batteries, J. Am. Chem. Soc. 139 (2017) 12710–12715.

[53] W. Chen, T. Lei, W. Lv, Y. Hu, Y. Yan, W. He, Z. Li, C. Yan, J. Xiong, Atomic interlamellar ion path in high sulfur content lithium-montmorillonite host enables high-rate and stable lithium–sulfur battery, Adv. Mater. 30 (2018) 1804084.

[54] H. Tian, Z. Li, G. Feng, Z. Yang, D. Fox, M. Wang, H. Zhou, L. Zhai, A. Kushima, Y. Du, Z. Feng, X. Shan, Y. Yang, Stable, high-performance, dendrite-free, seawater-based aqueous batteries, Nat. Commun. 12 (2021) 237.

[55] X. Yong, J. Wang, C. Liu, H. Wang, Y. Hong, G. Zheng, Z.W. Seh, Q. Cai, W. Li, G. Zhou, C. Zu, Y. Cui, Balancing surface adsorption and diffusion of lithium-polysulfides on nonconductive oxides for lithium–sulfur battery design, Nat. Commun. 7 (2016) 11203.

[56] Tao Chen, Weihua Kong, Zewen Zhang, Lei Wang, Yi Hu, Guoyin Zhu, Renpeng Chen, Lianbo Ma, Wen Yan, Yanrong Wang, Jie Liu, Zhong Jin, Ionic liquid-immobilized polymer gel electrolyte with self-healing capability, high ionic

conductivity and heat resistance for dendrite-free lithium metal batteries, Nano Energy 54 (2018) 17–25, https://doi.org/10.1016/j.nanoen.2018.09.059.
[57] Wen Yan, Jie Wei, Tao Chen, Lei Duan, Lei Wang, Xiaolan Xue, Renpeng Chen, Weihua Kong, Huinan Lin, Chenghui Li, Zhong Jin, Superstretchable, thermostable and ultrahigh-loading lithium–sulfur batteries based on nanostructural gel cathodes and gel electrolytes, Nano Energy 80 (2021) 105510, https://doi.org/10.1016/j.nanoen.2020.105510.
[58] Ning Ding, Sheau Wei Chien, T.S. Andy Hor, Zhaolin Liu, Yun Zong, Key parameters in design of lithium sulfur batteries, Journal of Power Sources 269 (2014) 111–116, https://doi.org/10.1016/j.jpowsour.2014.07.008.